JACS
JOURNAL OF THE AMERICAN CHEMICAL SOCIETY

Communication

pubs.acs.org/JACS

Spin State As a Probe of Vesicle Self-Assembly

Sanghoon Kim,[†] Christine Bellouard,*[,‡] Julian Eastoe,[§] Nadia Canilho,[†] Sarah E. Rogers,[∥] Dris Ihiawakrim,[⊥] Ovidiu Ersen,[⊥] and Andreea Pasc*[,†]

[†]SRSMC, UMR 7565, Université de Lorraine/CNRS, F-54506 Vandoeuvre-lès-Nancy, France

[‡]Institut Jean Lamour, UMR 7198, Université de Lorraine/CNRS, F-54506 Vandoeuvre-lès-Nancy, France

[§]School of Chemistry, University of Bristol, Cantock's Close, Bristol, BS8 1TS, U.K.

[∥]Rutherford Appleton Laboratory, ISIS Facility, Chilton, Oxfordshire OX11 0QX, U.K.

[⊥]Institut de Physique et Chimie des Matériaux de Strasbourg, UMR 7504 CNRS - Université de Strasbourg, 23 rue du Loess, BP 43, 67034 Strasbourg cedex 2, France

Supporting Information

ABSTRACT: A novel system of paramagnetic vesicles was designed using ion pairs of iron-containing surfactants. Unilamellar vesicles (diameter ≈ 200 nm) formed spontaneously and were characterized by cryogenic transmission electron microscopy, nanoparticle tracking analysis, and light and small-angle neutron scattering. Moreover, for the first time, it is shown that magnetization measurements can be used to investigate self-assembly of such functionalized systems, giving information on the vesicle compositions and distribution of surfactants between the bilayers and the aqueous bulk.

In recent years, vesicles have been widely studied for potential applications in diverse fields such as biomedicine,[1−4] catalysis,[5−7] and cosmetics.[8] Vesicles are spherical self-assembly systems comprising lipid bilayer membranes enclosing internal aqueous compartments. Since vesicles are structurally similar to biological membranes, they are considered as cell mimics.[9] Furthermore, vesicles are employed to encapsulate fragrances, flavors, or drugs for controlled release. Functional vesicles which respond to external stimuli such as temperature,[10] pH,[11,12] redox,[13,14] and magnetic field gradient,[15−17] have been widely studied as drug nanovectors.

In terms of triggerable systems, magnetic vesicles are of significant interest because magnetic properties can be beneficial in applications such as magnetic resonance imaging (MRI) or hyperthermia as well as spatial and temporal drug targeting.[18−21]

To generate magnetic vesicles, three approaches have been used to date: first, loading magnetic nanoparticles in the internal aqueous cores;[16,20−23] embedding nanoparticles within the hydrophobic tails of lipids in bilayers;[24,25] and finally, encapsulating nanoparticles between bilayers of multilamellar membranes.[26,27]

An alternative strategy is employed here, by introducing magnetic surfactants or lipids in the bilayers.

Recently, magneto-responsive surfactants (MagSurfs)[28] have been introduced opening up a range of interesting magnetic colloidal systems such as micelles,[29] emulsions,[30] solid lipid nanoparticles,[31] organosols,[32] or magnetized DNA.[33] These MagSurfs have also been used as structure directing agents for synthesis of magnetic mesoporous silica materials.[34] Here, for the first time, new paramagnetic vesicles are reported which can be readily generated from ion pairs of anionic and cationic iron surfactants. This strategy was inspired by the well-known catanionic surfactants[35−37] that spontaneously form vesicles in a range of anion/cation ratios (r) close to stoichiometry. Herein, by exploiting the paramagnetic properties of Fe^{3+}, it is possible to investigate more accurately the range of self-assembly of surfactant ion pairs into vesicles and to give a clear picture of the partitioning between vesicles and bulk.

The necessary Fe^{3+} MagSurfs can be prepared from conventional surfactants, cationic dodecyltrimethylammonium bromide (DTAB) and anionic sodium bis(2-ethylhexyl) sulfosuccinate (AOT) to afford DTAF and AOT_3F, respectively.

Scheme 1. Molecular Structures of MagSurfs (AOT_3F and DTAF)

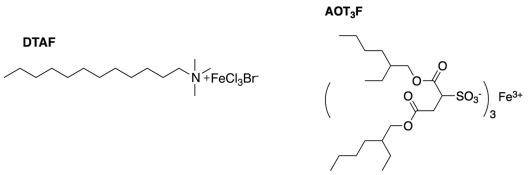

The behavior of these MagSurfs (AOT_3F, DTAF) in aqueous solutions is close to those of the parent surfactants. The single chain DTAF has a critical micelle concentration (CMC) of 13.6 mM at 25 °C, which is similar to that of DTAB (15.5 mM).[28] However, its melting point decreases from 246 to 32 °C. The critical micelle concentration of AOT_3F is 2.2 mM (with respect to AOT moiety, or 0.7 mM with respect to AOT_3F), which is also close to the CMC of the parent surfactant, AOT (~2.5 mM).[38]

Two series of four systems denoted Ax and Bx (with x = 1, 2, 3, 4) have been prepared. A and B stand for two different surfactant concentration ratios $r = C_{DATF}/C_{AOT_3F}$: 3.7 and 8.1 respectively. These ratios were chosen in order to investigate both the self-assembly near stoichiometry between ionic pairs (3.7) and far from equimolarity, in a system rich in DTAF. The total surfactant

Received: January 15, 2016
Published: February 9, 2016

DOI: 10.1021/jacs.6b00537
J. Am. Chem. Soc. 2016, 138, 2552−2555

concentrations of A1 and B1 are respectively 21.4 and 15.2 mM. Then, these systems were diluted 2-fold from A*x*-1 (B*x*-1) to A*x* (B*x*), where $x > 1$ is then the number of 2-fold dilutions of A1 (B1).

Gentle mixing of both surfactants results in vesicle formation, as shown in Figure 1a and b by cryogenic transmission electron

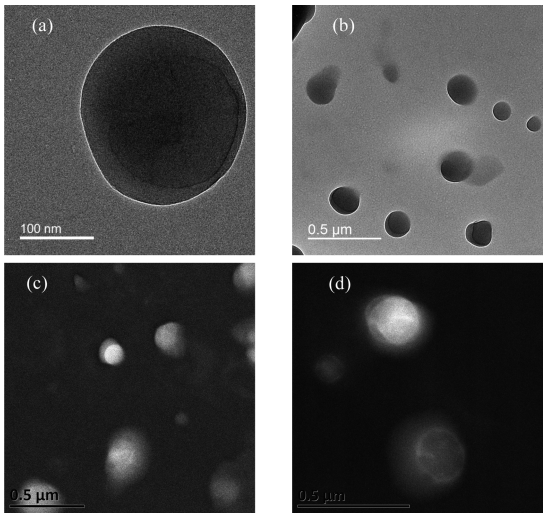

Figure 1. Cryo-TEM images of vesicles observed for systems A2 (a) and A3 (b); Cryo-STEM images of vesicles observed for systems A2 (c) and B2 (d).

microscopy (Cryo-TEM) and in Figure 1c and d by scanning transmission electron microscopy (Cryo-STEM). The conditions of these Cryo-TEM experiments are similar to those for the magnetic measurements. For both techniques, the visualized vesicles have sizes of about 200 nm. However, smaller vesicles of about 100 nm were also observed (Figures 1b,c and S1). It should be noted that these vesicles are out-of-equilibrium systems, and therefore the vesicles are not perfectly monodisperse. Interestingly, the Cryo-STEM offers further insights into the vesicle structures. For example, Figure 1d shows (upper) a top view of a vesicle showing an almost identical phase contrast and (lower) an inside view of the vesicle showing the hollow structure.

Dynamic light scattering (DLS) measurements and nanoparticle tracking analysis (NTA) allow for further characterization of the size distributions (Figure 2) from different perspectives. For both series (A1 and B1), the size distributions from DLS are centered at ~200 nm. Moreover, as shown in Figure S2, the size distribution does not depend on the composition ratio *r*. The size distribution observed by NTA exhibits a shoulder for smaller sizes (around roughly 100 nm), which are also present in TEM and STEM images, but are

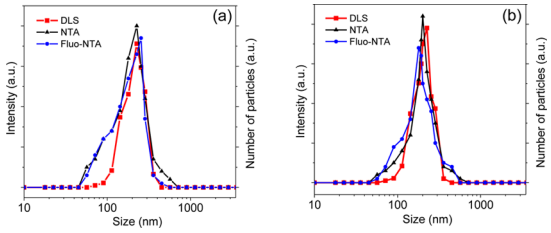

Figure 2. Size distribution of MagSurf vesicles measured for A1 (a) and B1 (b), using DLS (red, ■), NTA (black, ▲), and NTA with fluorescence filter blue, ●).

difficult to see by DLS (owing to the much more highly scattering larger population). Moreover, the use of a fluorescence filter with NTA allows detection of fluorescent aggregates containing iron ions (video in SI). This is direct proof that the iron counterions are in the vesicle hydration shells.

The structures of these magnetic vesicles were also investigated using small-angle neutron scattering (SANS). Vesicle samples were prepared in D_2O in order to enhance the neutron scattering contrast. Figure 3a and b show SANS

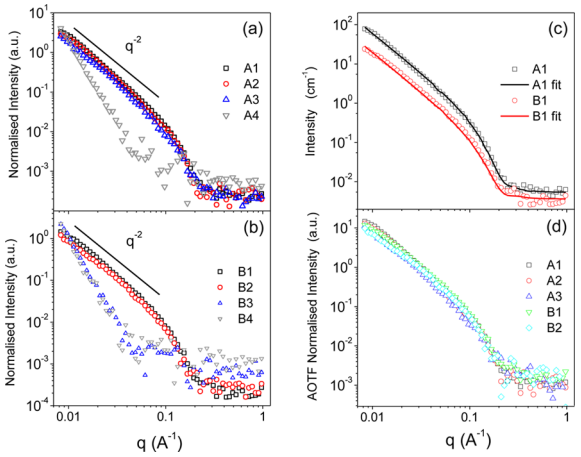

Figure 3. Small-angle neutron scattering data normalized to total molar MagSurf concentration for A*x* (a), B*x* (b), fitted data for A1 and B1 (c), normalized SANS data with respect to AOT_3F concentration for A1−3 and B1−2 (d).

intensities $I(q)$ for the A*x* and B*x* series as a function of scattering vector q; the curves have been normalized with respect to the total surfactant concentration C_T (Table S1). For the A1 to 3 and B1 to 2 samples, the low q regions exhibit a clear q^{-2} decays, which is a general feature of SANS from locally planar surface structures, such as bilayers or vesicles.[39] In addition, the normalized SANS data for A1 to 3 (Figure 3a) and B1 to 2 (Figure 3b) show a common q dependence, indicating that the vesicles have similar, concentration-independent structures. The SANS data were fitted using a noninteracting polydisperse vesicle form factor model (Sasview[40] HardsphereStructure for P(Q)*S(Q)). The $I(q)$ profiles from all samples A1 to 3, B1 to 2 are well described by this model, as illustrated in Figure 3c for A1 and B1. The shell thicknesses τ were approximately 2.5 nm (Table S1). The fitted values for τ suggest the vesicles are unilamellar, since 2.5 nm corresponds to 2 × C12 disordered alkyl chain lengths. All parameters deduced from DLS and SANS are very similar for the A and B series (Table S1); moreover, the concentration-normalized $I(q)$ superimposes as a function of AOT concentration (Figure 3d). This shows that the vesicles are not affected by the ratio r and that vesicle concentration is proportional to AOT_3F concentration for both r ratios. The abrupt change in $I(q)$ observed between A3 and A4 (Figure 3a) and between B2 and B3 (Figure 3b) indicates a transition from vesicles toward less well-defined aggregates on dilution. The critical vesicle concentrations (CVCs) can be estimated from these dilution series of $I(q)$: CVC is between 5.4 and 2.7 mM (1.13 and 0.56 mM AOT_3F) for the DTAF/AOT_3F ratio r of 3.7 and between 7.6 and 3.8 mM (0.84 and 0.42 mM AOT_3F) for DTAF/AOT_3F for $r = 8.1$.

On the other hand, the critical aggregation concentration (CAC) was estimated using surface tension measurements

DOI: 10.1021/jacs.6b00537
J. Am. Chem. Soc. 2016, 138, 2552−2555

(Figure S3). The CAC value, expressed as a function of AOT_3F concentration, is essentially identical for both DTAF/AOT_3F ratios: about 1.5×10^{-2} mM which corresponds to a total surfactant concentration of 7×10^{-2} mM for $r = 3.7$ and about 0.13 mM for $r = 8.1$.

All these results suggest that the self-assembly mechanism of AOT_3F and DTAF ion pairs with increasing concentration in aqueous dispersions involves a transition from primary mixed aggregates to vesicles. This behavior was already observed for catanionic surfactants that also undergo vesicle formation.[41,42] However, to date no clear evidence of the composition of the vesicle bilayers as well as on the distribution of the surfactants between the bilayers and the bulk has been presented. This is done here, by taking advantage of the paramagnetic properties of these MagSurfs: magnetic measurements were performed at low temperature.

Figure 4a and b present the temperature dependence of magnetization measured in an applied field of 70 kOe for the A and B series respectively. Interestingly, these curves exhibit qualitative behavior which correlates with the SANS data (Figure 3a and b): magnetization of A1−3 and B1−2 reported per Fe weight are almost superimposed as were SANS data, whereas a notable decrease is clearly observed on further dilution, from A3 to A4, and B2 to B3, as the vesicles are disrupted. Moreover, the measured magnetization at low temperature of A1−3 (≈ 420 emu/g) is quite close to the saturation magnetization of Fe^{3+} ions with $S = 5/2$ ($M_s^{5/2} = 500$ emu/g_{Fe}) whereas it is much lower for B1−2 (≈ 300 emu/g), which has a lower vesicle concentration. The decrease in signal observed after vesicle breakup (from A3 to A4, or B2 to B3) or with decreasing vesicle concentration (from A1−3 to B1−2) is attributed to an Fe^{3+} spin crossover from high spin (5/2) to low spin state (1/2).

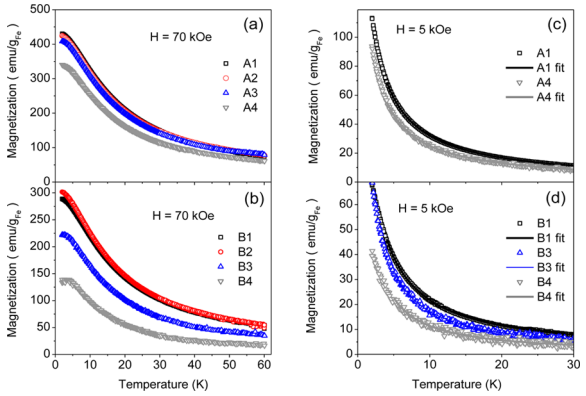

Figure 4. Magnetization measurements as a function of temperature at 70 kOe for A1−4 (a), B1−4 (b), at 5 kOe for A1 and 4 (c) ; B1 and 3−4 (d). The lines in plots (c) and (d) are fits with a sum of two Brillouin functions as described in the text.

To obtain the fraction of high spins with respect to low spins, the low field (H= 5 kOe) temperature magnetization has been fitted with the contribution of two Brillouin functions as described in Supporting Information. The lines in Figure 4c and d correspond to the sum of the Brillouin functions with fitted parameters. The fraction of spins 5/2, $f_{5/2}$, is reported in Table S1. Interestingly, the highest $f_{5/2}$ (≈ 90−87%) is found for A1−3, which contain a larger vesicle concentration.

The presence of high spin state can be associated with long-range intermolecular associations, such as that found in vesicles, and low spin state (S = 1/2) to Fe sites interacting with water, as expected at the edges of membrane fragments, or in free nonaggregated monomers. Spin crossover (SCO) of a complex compound in the bulk solid state is generally studied as a function of an external parameter, such as temperature, pressure, and light exposure.[43] Moreover, in nanomaterials the size reduction can provide an additional tool to tune the SCO.[44] In the liquid state, it has been shown that a hysteretic spin transition can be induced in a solution assembly of an Fe^{3+} amphiphilic complex.[45,46] Here, the different spin states result from the presence or absence of molecular autoassembly in water, depending on the surfactant concentrations. When involved in vesicles, the $FeCl_3Br^-$ anions are less exposed to water than non-self-assembled monomers,[28] for which hydrogen bonding with the anion may occur, inducing a reduction of the molecular volume and a low spin state below the freezing temperature.

To support this, magnetic measurements have been performed with pure DATF and AOT_3F (1.47 and 0.50 mM respectively) where free monomers dominate below the CMCs (which are 13.6 and 0.73 mM respectively). Results are reported in Figures S4 and S5. For both surfactants, the high spin concentration is close to 30−40%, which attributes spin 1/2 to monomers only.

To investigate the distribution of surfactants in vesicles, magnetic measurements have been also performed as a function of surfactant ratio r, for a constant total surfactant concentration (equal that in A3). The fraction of high spin $f_{5/2}$, plotted in Figure 5, presents a smooth maximum for r between 3 and 4 and decreases below $r \approx 3$ and above $r \approx 4$. The decrease of $f_{5/2}$ above $r \approx 4$ corroborates the results obtained for A and B systems: in this ratio range, the vesicle concentration is limited by the AOT_3F concentration, and the additional proportion of DTAF is not involved in vesicles but is lost as monomers (or low spins), or as micelles for higher DTAF excess. Below $r \approx 3$, one could expect that the vesicle concentration is limited by the DTAF concentration, and then monomers of AOT_3F provide a low spin signal. This figure shows that despite vesicles existing over a wide range of surfactant concentration ratios, the ratio range for high spin vesicles is roughly between 3 and 4 DTAF molecules per AOT_3F. As a result, vesicles of DTAF/AOT_3F result from an ordered molecular arrangement.

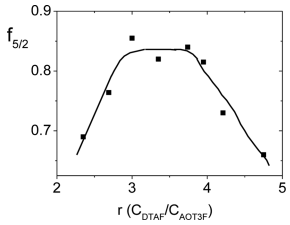

Figure 5. High spin fraction $f_{5/2}$ as a function of the ratio "r" of DTAF and AOT_3F concentrations; the total surfactant concentration has been kept constant and equal to 5.4 mM.

In conclusion, we show that the self-assembly of surfactants can be investigated through the spin state of the metallic centers (Figure 6). Moreover, with this tool, one can assess the critical vesicle concentration and the partitioning of surfactants between bilayers and free in solution. This key property of vesicle systems cannot be addressed with techniques previously employed; therefore, the approach described here is unique and is expected to provide new insight into vesicle self-assembly.

DOI: 10.1021/jacs.6b00537
J. Am. Chem. Soc. 2016, 138, 2552−2555

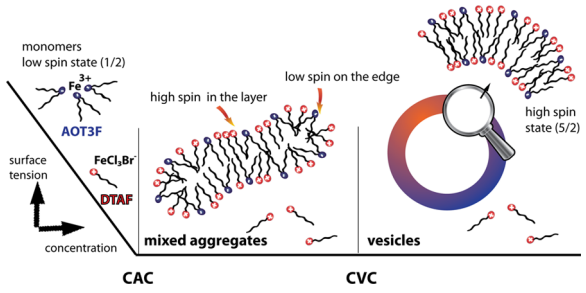

Figure 6. Schematic representation showing the spin crossover of self-assembled MagSurfs: low spin in monomers, low spin and high spin in bilayers and high spin in vesicles.

■ ASSOCIATED CONTENT

Supporting Information

The Supporting Information is available free of charge on the ACS Publications website at DOI: 10.1021/jacs.6b00537.

Details on the synthesis and self-assembly characterization (Cryo-TEM, -STEM, DLS, NTA, SANS, surface tension and magnetic measurements) of surfactants (PDF)
Videos of A1 and B1 with and without a filter (ZIP)

■ AUTHOR INFORMATION

Corresponding Authors

*christine.bellouard@univ-lorraine.fr
*andreea.pasc@univ-lorraine.fr

Notes

The authors declare no competing financial interest.

■ ACKNOWLEDGMENTS

The authors thank the UK Science and Technology Facilities Council (STFC) for allocation of beamtime at ISIS and grants toward consumables and travel. Financial support was received from Institut Jean Barriol and CNRS/University of Lorraine (Project CaMéLIA, PEPS Mirabelle 2014). S.K. acknowledges the French Minister for Research and Education for the Ph.D. grant. A.P. acknowledges COST CM1101 network for the STSM grant.

■ REFERENCES

(1) Kumar, G. P.; Rajeshwarrao, P. *Acta Pharm. Sin. B* **2011**, *1*, 208.
(2) Sinico, C.; Fadda, A. M *Expert Opin. Drug Delivery* **2009**, *6*, 813.
(3) Yuk, S. H.; Oh, K. S.; Koo, H.; Jeon, H.; Kim, K.; Kwon, I. C. *Biomaterials* **2011**, *32*, 7924.
(4) Brinkhuis, R. P.; Rutjes, F. P. J. T.; van Hest, J. C. M. *Polym. Chem.* **2011**, *2*, 1449.
(5) Debecker, D. P.; Faure, C.; Meyre, M.-E.; Derré, A.; Gaigneaux, E. M. *Small* **2008**, *4*, 1806.
(6) Watanabe, K.; Takizawa, S.-Y.; Murata, S. *Chem. Lett.* **2011**, *40*, 345.
(7) Adamala, K.; Szostak, J. W. *Nat. Chem.* **2013**, *5*, 495.
(8) Al Bawab, A.; Heldt, N.; Li, Y. *J. Dispersion Sci. Technol.* **2005**, *26*, 251.
(9) Walde, P. *BioEssays* **2010**, *32*, 296.
(10) Zhou, C.; Cheng, X.; Yan, Y.; Wang, J.; Huang, J. *Langmuir* **2014**, *30*, 3381.
(11) Du, J.; Tang, Y.; Lewis, A. L.; Armes, S. P. *J. Am. Chem. Soc.* **2005**, *127*, 17982.
(12) Wang, H.; Xu, F.; Wang, Y.; Liu, X.; Jin, Q.; Ji, J. *Polym. Chem.* **2013**, *4*, 3012.
(13) Ren, T.-B.; Feng, Y.; Zhang, Z.-H.; Li, L.; Li, Y.-Y. *Soft Matter* **2011**, *7*, 2329.
(14) Li, Q.; Chen, X.; Jing, B.; Zhao, Y.; Ma, F. *Colloids Surf., A* **2010**, *355*, 146.
(15) Lecommandoux, S.; Sandre, O.; Chécot, F.; Rodriguez-Hernandez, J.; Perzynski, R. *Adv. Mater.* **2005**, *17*, 712.
(16) Beaune, G.; Dubertret, B.; Clément, O.; Vayssettes, C.; Cabuil, V.; Ménager, C. *Angew. Chem., Int. Ed.* **2007**, *46*, 5421.
(17) Ye, F.; Barrefelt, Å.; Asem, H.; Abedi-Valugerdi, M.; El-Serafi, I.; Saghafian, M.; Abu-Salah, K.; Alrokayan, S.; Muhammed, M.; Hassan, M. *Biomaterials* **2014**, *35*, 3885.
(18) Sanson, C.; Diou, O.; Thévenot, J.; Ibarboure, E.; Soum, A.; Brûlet, A.; Miraux, S.; Thiaudière, E.; Tan, S.; Brisson, A.; Dupuis, V.; Sandre, O.; Lecommandoux, S. *ACS Nano* **2011**, *5*, 1122.
(19) Niu, D.; Wang, X.; Li, Y.; Zheng, Y.; Li, F.; Chen, H.; Gu, J.; Zhao, W.; Shi, J. *Adv. Mater.* **2013**, *25*, 2686.
(20) Martina, M-S.; Fortin, J-P.; Ménager, C.; Clément, O.; Barratt, G.; Grabielle-Madelmont, C.; Gazeau, F.; Cabuil, V.; Lesieur, S. *J. Am. Chem. Soc.* **2005**, *127*, 10676.
(21) Béalle, G.; Di Corato, R.; Kolosnjaj-Tabi, J.; Dupuis, V.; Clément, O.; Gazeau, F.; Wilhelm, C.; Ménager, C. *Langmuir* **2012**, *28*, 11834.
(22) Yang, X.; Pilla, S.; Grailer, J. J.; Steeber, D. A.; Gong, S.; Chen, Y.; Chen, G. *J. Mater. Chem.* **2009**, *19*, 5812.
(23) Yang, X.; Grailer, J. J.; Rowland, I. J.; Javadi, A.; Hurley, S. A.; Matson, V. Z.; Steeber, D. A.; Gong, S. *ACS Nano* **2010**, *4*, 6805.
(24) Arosio, P.; Thévenot, J.; Orlando, T.; Orsini, F.; Corti, M.; Mariani, M.; Bordonali, L.; Innocenti, C.; Sangregorio, C.; Oliveira, H.; Lecommandoux, S.; Lascialfari, A.; Sandre, O. *J. Mater. Chem. B* **2013**, *1*, 5317.
(25) Zhou, J.; Chen, M.; Diao, G. *ACS Appl. Mater. Interfaces* **2014**, *6*, 18538.
(26) Meyre, M.-E.; Clérac, R.; Mornet, S.; Duguet, E.; Dole, F.; Nallet, F.; Lambert, O.; Trépout, S.; Faure, C. *Phys. Chem. Chem. Phys.* **2010**, *12*, 12794.
(27) Krack, M.; Hohenberg, H.; Kornowski, A.; Lindner, P.; Weller, H.; Förster, S. *J. Am. Chem. Soc.* **2008**, *130*, 7315.
(28) Brown, P.; Bushmelev, A.; Butts, C. P.; Cheng, J.; Eastoe, J.; Grillo, I.; Heenan, R. K.; Schmidt, A. M. *Angew. Chem., Int. Ed.* **2012**, *51*, 2414.
(29) Brown, P.; Bushmelev, A.; Butts, C. P.; Eloi, J.-C.; Grillo, I.; Baker, P. J.; Schmidt, A. M.; Eastoe, J. *Langmuir* **2013**, *29*, 3246.
(30) Brown, P.; Butts, C. P.; Eastoe, J.; Glatzel, S.; Grillo, I.; Hall, S. H.; Rogers, S.; Trickett, K. *Soft Matter* **2012**, *8*, 11609.
(31) Kim, S.; Durand, P.; Roques-Carmes, T.; Eastoe, J.; Pasc, A. *Langmuir* **2015**, *31*, 1842.
(32) Smith, G. N.; Eastoe, J. *J. Colloid Interface Sci.* **2014**, *426*, 252.
(33) Brown, P.; Khan, A. M.; Armstrong, J. P. K.; Perriman, A. W.; Butts, C. P.; Eastoe, J. *Adv. Mater.* **2012**, *24*, 6244.
(34) Kim, S.; Bellouard, C.; Pasc, A.; Lamouroux, E.; Blin, J.-L.; Carteret, C.; Fort, Y.; Emo, M.; Durand, P.; Stébé, M.-J. *J. Mater. Chem. C* **2013**, *1*, 6930.
(35) Michina, Y.; Carrière, D.; Mariet, C.; Moskura, M.; Berthault, P.; Belloni, L.; Zemb, T. *Langmuir* **2009**, *25*, 698.
(36) Béalle, G.; Jestin, J.; Carrière, D. *Soft Matter* **2011**, *7*, 1084.
(37) Noirjean, C.; Testard, F.; Jestin, J.; Taché, O.; Dejugnat, C.; Carriere, D. *Soft Matter* **2014**, *10*, 5928.
(38) Lin, C.; Zhao, J.; Jiang, R. *Chem. Phys. Lett.* **2008**, *464*, 77.
(39) Hubbard, F. P.; Santonicola, G.; Kaler, E. W.; Abbott, N. L. *Langmuir* **2005**, *21*, 6131.
(40) http://www.sasview.org/index.html.
(41) Shioi, A.; Hatton, T. A. *Langmuir* **2002**, *18*, 7341.
(42) O'Connor, A. J.; Hatton, T. A.; Bose, A. *Langmuir* **1997**, *13*, 6931.
(43) Brooker, S. *Chem. Soc. Rev.* **2015**, *44*, 2880.
(44) Salmon, L.; Molnar, G.; Zitouni, D.; Quintero, C.; Bergaud, C.; Micheau, J.-P.; Bousseksou, A. *J. Mater. Chem.* **2010**, *20*, 5499.
(45) Gaspar, A. B.; Seredyuk, M. *Coord. Chem. Rev.* **2014**, *268*, 41.
(46) Gandolfi, C.; Morgan, G. G.; Albrecht, M. *Dalton Trans.* **2012**, *41*, 3726.

DOI: 10.1021/jacs.6b00537
J. Am. Chem. Soc. 2016, 138, 2552−2555